





Signal-to-noise Ratio Analytic Formulae of the Inspiral Binary Black Holes in TianQin

Hong-Yu Chen(陈洪昱), Han Wang(王晗), En-Kun Li(李恩坤),* and Yi-Ming Hu(胡一鸣)[†]

MOE Key Laboratory of TianQin Mission, TianQin Research Center

for Gravitational Physics & School of Physics and Astronomy,

Frontiers Science Center for TianQin, Gravitational Wave Research Center of CNSA,

Sun Yat-sen University (Zhuhai Campus), Zhuhai, 519082, China

(Dated: December 11, 2024)

Binary black holes are one of the important sources for the TianQin gravitational wave project. Our research has revealed that, for TianQin, the signal-to-noise ratio of inspiral binary black holes can be computed analytically. This finding is expected to greatly simplify the estimation of detection capabilities for binary black holes. In this paper, we demonstrated the signal-to-noise ratio relationships from stellar-mass black holes to massive black holes. With the all-sky average condition, the signal-to-noise ratio for most binary black hole signals can be determined with a relative error of $\lesssim 10\%$, with notable deviations only for chirp masses near $1000 M_{\odot}$. In contrast, the signal-to-noise ratio without the average includes an additional term, which we refer to as the response factor. Although this term is not easily calculated analytically, we provide a straightforward estimation method with an error margin of 1σ within 2%.

I. INTRODUCTION

In recent years, the domain of gravitational wave (GW) detection has undergone remarkable advancements, marking a significant milestone in the scientific community. One of the key breakthroughs came in 2015, when Laser Interferometer GW Observatory (LIGO) [1] successfully detected the first GW signal from a binary black hole (BBH) merger [2, 3]. So far, nearly a hundred of GW detections have been officially announced by ground-based detectors [4–6]. Furthermore, evidence for the stochastic GW background has recently been reported by pulsar timing array (PTA) [7–10]. In parallel, research on space-based GW detectors is also progressing [11]. For example, the TianQin project [12], a space-borne GW detection mission, aims to detect low-frequency GWs and further advance our understanding of the universe[13].

TianQin consists of three satellites positioned in a geostationary orbit approximately 100,000 kilometers above the Earth's surface, forming an equilateral triangle. These satellites emit and receive laser beams among themselves, effectively creating a space-based laser interferometer. The principle of the TianQin detector lies in measuring minor variations in the distances between the satellites, which are caused by the passing of GWs. Influenced by the laser arm length and various instrumental noise factors of TianQin, the detector's sensitive frequency band ranges from 0.1 mHz to 1 Hz. One of the main sources for TianQin is the BBH. TianQin is expected to be capable of observing BBH systems across cosmic history, from the early universe (with a redshift of approximately $z \sim 20$) to the present era [14]. In this paper, we will discuss the massive black hole bi-

nary (MBHB) and stellar mass binary black hole (SBBH) systems separately.

MBHB, as one of the most intense cosmic phenomena, is expected to accumulate sufficient signal-to-noise ratio (SNR) on the TianQin detector during the inspiral phase, making it detectable before the merger. This capability presents us with a unique astrophysical laboratory to delve into the formation and evolution of black holes [15, 16], trace the history of the cosmos [15, 17], and test gravitational theories [18–20]. Moreover, the early warnings of MBHB systems before their merger could significantly advance the field of multi-messenger astronomy [21]. We have found that due to the unique sensitivity curve of TianQin, the SNR of GWs emitted by inspiral MBHBs follows a special relationship:

$$\rho^2 \propto \frac{\text{observation time}}{\text{time to coalescence}} \quad (1)$$

For SBBHs, they merge at high frequencies, space-based GW detectors can observe their early inspiral phase within the lower frequency range. The detection of SBBHs in the millihertz band with a long observation time enables more precise measurements of parameters such as mass and sky location, while also preserving the evolution of key properties such as eccentricity and spin [22, 23]. These capabilities not only help constrain the formation mechanisms of such systems [24, 25], but also facilitate measuring the Hubble parameter or constraining certain parameters in modified gravity theories with great precision [26–29]. We have found that, for TianQin, the SNR of GWs emitted by inspiral SBBHs follows a special relationship:

$$\rho^2 \propto \sqrt{\text{observation time}} - \sqrt{\text{time to coalescence}} \quad (2)$$

These relationships will significantly facilitate the estimation of the SNR for the inspiral phase of BBHs, as well as the forecast of detection capabilities before coalescence. In this work, we will conduct a more detailed derivation and discussion of these relationships.

* lienk@sysu.edu.cn

[†] huyiming@sysu.edu.cn

Section II will outline the formula for calculating the SNR. Sections III explore the SNR accumulation for MBHB systems in the TianQin detector, under All-Sky Average (ASA) and non-average conditions respectively. Then, Sections IV delves into the feasibility of formulating an analytical SNR formula for the inspiral SBBHs. We conclude with a summary in Section V.

II. SNR CALCULATION

The SNR can be described as the ratio of the signal amplitude to the sensitivity of the detector. The optimal SNR is commonly computed using the inner product approach [30, 31]:

$$\rho = \sqrt{\langle h | h \rangle}, \quad (3)$$

where h is the waveform of the signal, and $\langle a | b \rangle$ represents the inner product between a and b expressed as follows:

$$\langle a | b \rangle = 4\Re \int_0^\infty \frac{\tilde{a}(f) \cdot \tilde{b}^*(f)}{S_n(f)} df, \quad (4)$$

where $S_n(f)$ is the one-sided noise power spectral density (PSD) and \Re is the real component. The instrument settings used for the TianQin/LISA PSD are detailed in Appendix A.

During the inspiral phase, BBH signals can be accurately approximated using post-Newtonian formulae [32], under which the frequency can be expressed as a function of observation time:

$$f(t) = \frac{1}{8\pi} \left(\frac{GM}{c^3} \right)^{-5/8} \left(\frac{t_c - t}{5} \right)^{-3/8}. \quad (5)$$

Here, G and c denote the gravitational constant and the speed of light, t_c and \mathcal{M} correspond to the coalescence time and the detector-frame chirp mass. Setting the time origin at the onset of the observation period, the upper and lower limits of the frequency of the SNR integration are $f_{\max} = f(T_{\text{obs}})$ and $f_{\min} = f(0)$, respectively. Moreover, we need to cutoff the data to reduce errors if the signal frequency exceeds the cutoff frequency of TianQin. A detailed description can be found in the Appendix A.

In the computation of the optimal SNR, we solely utilize the real component of the inner product. As a result, the phase of the waveform has a negligible impact on the calculation of the SNR, enabling us to ascertain the SNR value purely based on the waveform's amplitude. The amplitude of GW emitted by inspiral BBH systems can be represented by a simple post-Newtonian formula [33]:

$$\mathcal{A}(f) = \sqrt{\frac{2}{3\pi^{1/3}}} c^{-3/2} \frac{1}{D_L} (GM)^{5/6} f^{-7/6}, \quad (6)$$

where D_L represents the luminosity distance. After the frequency band and amplitude are known, calculating the

SNR involves computing the response function and the noise PSD. Next, we will specifically introduce the accumulation relationship of SNR over time under both ASA and non-average scenarios.

III. MASSIVE BLACK HOLES

A. All-Sky Average

By using low-frequency approximation, we can provide the analytic formula of the SNR for the TianQin detector's observation of inspiral MBHBs:

$$\begin{aligned} \rho(T_{\text{obs}}) &= \sqrt{\frac{15}{2048}} \frac{L}{D_L} \frac{c}{\sqrt{N_a t_c}} \times \sqrt{\frac{t_{\text{obs}}}{t_c - t_{\text{obs}}}}, \\ &\approx 185.2 \times \frac{1 \text{ Gpc}}{D_L} \sqrt{\frac{1 \text{ week}}{t_c}} \times \sqrt{\frac{T_{\text{obs}}}{t_c - T_{\text{obs}}}}, \end{aligned} \quad (7)$$

A detailed description of the calculation process can be found in the Appendix B.

To verify the precision of the estimation formula, we examined the error levels across different chirp masses and observation times. In our test, all the BBH systems are merged at the third month mark ($t_c = 3$ months), and the true signal is generated by IMRPhenomD waveform [34, 35]. As depicted in Figure 1(a), for signals with chirp mass range from 10^3 to $10^4 M_\odot$, the relative error is minimal. Signals outside this region will be overestimated by our formula. Considering the low SNR of the inspiral BBHs, the deviation caused by this relative error will be very low, ensuring the reliability of the formula.

Next, we consider the lowest-order correction to obtain more accurate results:

$$\rho_{\text{corr}}^2 = \rho^2 + C, \quad (8)$$

where

$$\begin{aligned} C_{TQ} &= -\frac{3\pi c^{1/8}}{320000 \times 5^{3/8}} (GM)^{5/8} \left(\frac{L}{D_L} \right)^2 \frac{1}{N_a} \\ &\quad \times \left[(t_c - t_{\text{obs}})^{-5/8} - t_c^{-5/8} \right], \\ &\approx -1692 \left(\frac{\mathcal{M}}{10^4 M_\odot} \right)^{5/8} \left(\frac{1 \text{ Gpc}}{D_L} \right)^2 \\ &\quad \times \left[\left(\frac{t_c - T_{\text{obs}}}{1 \text{ week}} \right)^{-5/8} - \left(\frac{t_c}{1 \text{ week}} \right)^{-5/8} \right]. \end{aligned} \quad (9)$$

Figure 1(b) illustrates the improvement brought by this correction. Compared to Figure 1(a), the corrected SNR formula provides an accurate estimation for sources within the mass range of 10^3 to $10^5 M_\odot$. Signals with masses falling below this range are prone to be overestimated by our formula, whereas signals with masses exceeding this range are susceptible to underestimation. Systems with $\mathcal{M} \leq 10^3 M_\odot$ retain relatively poor estimation because the low-frequency approximation we used here is no longer suitable for these systems.

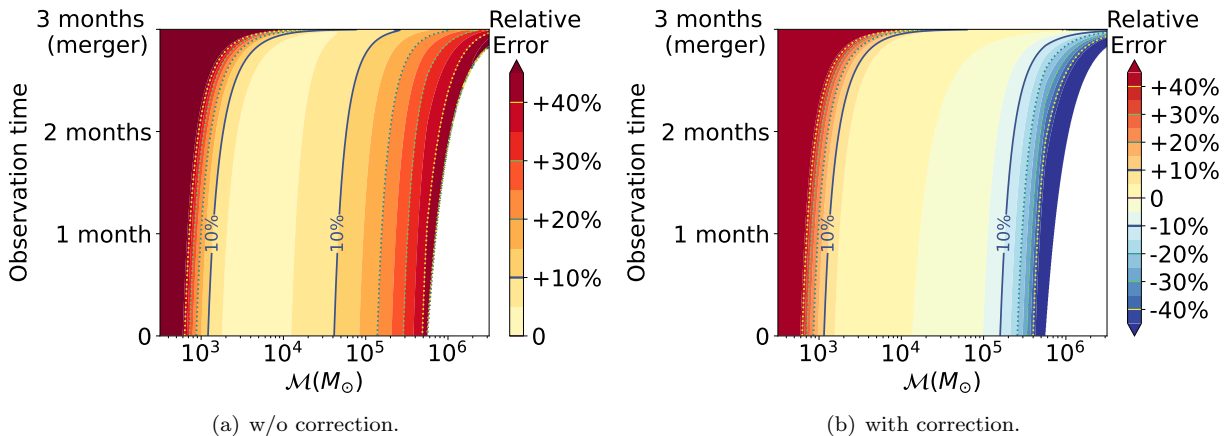


FIG. 1. Estimated error of the SNR for signals that merge at the third month, under different observation times and chirp mass conditions. The left and right panels respectively illustrate the estimated errors of Equation 7 and (8). The blank area in the lower right corner indicates that the signal has not yet entered the sensitive frequency band of TianQin.

We’ve also noted that this formula might not be well-suited for other space-based GW detectors, such as Laser Interferometer Space Antenna (LISA) [36]. LISA, which will be placed in heliocentric orbit, consists of three spacecraft forming an equilateral triangle with each arm spanning 2.5 million kilometers. The ASA sensitivity curve of LISA aligns with that of TianQin, differing only in arm length and two noise terms, as detailed in Appendix A. The increase in arm length enhances sensitivity in the low-frequency band, prompting us to select a lower cutoff frequency for LISA at 10^{-5} Hz rather than 10^{-4} for TianQin. Different dependencies of S_a on frequency only alter the higher-order terms of the SNR formula. For LISA, the lowest-order correction is:

$$\begin{aligned}
 C_{LISA} &= -\frac{3\pi^2}{2 \times 10^6 \times (5c)^{7/4}} (GM)^{5/4} \left(\frac{L}{D_L}\right)^2 \frac{1}{N_a} \\
 &\quad \times \left[(t_c - T_{\text{obs}})^{-1/4} - t_c^{-1/4} \right], \\
 &\approx -48298 \left(\frac{M}{10^4 M_\odot}\right)^{5/4} \left(\frac{1 \text{ Gpc}}{D_L}\right)^2 \\
 &\quad \times \left[\left(\frac{t_c - T_{\text{obs}}}{1 \text{ week}}\right)^{-1/4} - \left(\frac{t_c}{1 \text{ week}}\right)^{-1/4} \right] \quad (10)
 \end{aligned}$$

However, as shown in Figure 2, the estimated results of the SNR formula always have significant errors, regardless of whether the lowest-order correction is taken into account. The main reason is that the higher-order corrections in the LISA SNR formula are not negligible quantities. When not considering the lowest-order correction, as shown in Figure 2(a), the estimated error remains above 10%. Even with the lowest-order correction, only sources with masses around $3 \times 10^4 M_\odot$ can be estimated accurately. Furthermore, we attempted to vary the cutoff frequencies for LISA, with the low-frequency cutoff ranging from 10^{-5} Hz to 10^{-4} Hz, and the high-frequency cutoff ranging from 0.1 Hz to 1 Hz. Our find-

ings indicate that there is no substantial difference in the magnitude of estimation errors.

B. Non-average

The ASA result yields a mere approximation of expected values. The SNR of GW sources can vary greatly depending on their sky positions (latitude and longitude) and polar angles (polarization and inclination angle) in actual detection. We found that after considering the response, the estimated SNR is only multiplied by a factor compared to the ASA case, i.e.

$$\rho(T_{\text{obs}}) = P_{\text{res}} \times \rho_{\text{ASA}}(T_{\text{obs}}), \quad (11)$$

where the response factor P_{res} is a function of the sky position and polar angles, defined as:

$$P_{\text{res}}^2 = \frac{8\pi}{9} (P_{12}^2 + P_{23}^2 + P_{31}^2 - P_{12}P_{31} - P_{23}P_{31} - P_{12}P_{23}). \quad (12)$$

The expression $P_{ab} = n_l \cdot P^{22} \cdot n_l$ defines the inner product of the 2-2 mode polarization tensor P^{22} and the link unit vectors n_l between two satellites a and b . A detailed description of the calculation process can be found in the Appendix C.

Figure 3 illustrates the variation of the response factor across different sky positions and polar angles. Given the response factor’s dependence on all four positional angles, we integrate the remaining two angles to ascertain their relationship with a pair of selected angles during the computation process. As shown in Figure 3(a), the TianQin constellation exhibits pronounced sensitivity towards the double white dwarf system RX J0806.3 + 1527 (hereafter J0806) and the reciprocal direction, attributable to its orbital plane’s always facing the J0806. The orbital plane of TianQin and the coordinates of J0806 in the

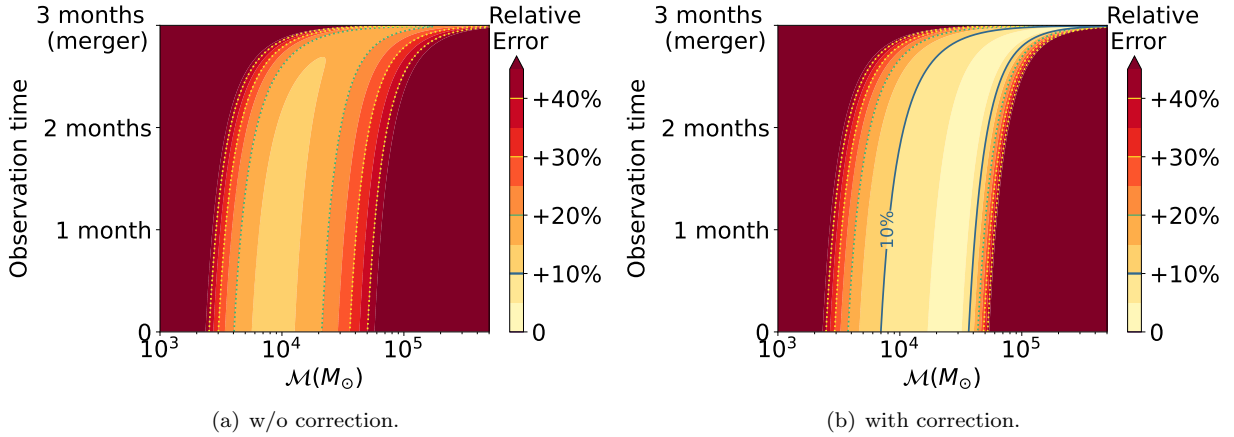


FIG. 2. The SNR estimation error for LISA varies with the chirp mass and observation time. The left panel uses the simplest zeroth-order SNR formula for estimation, while the right panel takes into account the lowest-order correction.

ecliptic reference frame are marked using red dashed line and red asterisk, respectively. In Figure 3(b), it is evident that the inclination angle ι has a more significant impact on the SNR compared to the polarization angle ψ . The SNR is maximized when the inclination angle approaches 0 or π , indicating that the detector is face-on the source. Conversely, the SNR is minimal when the inclination angle is near $\pi/2$, and it is under this condition that the polarization angle exerts a noticeable influence on the SNR. In contrast, at the poles of Figure 3(b), the contour lines are almost coincident with the lines of latitude, indicating that the influence of the polarization angle ψ can be disregarded in this area.

Although the response factor is challenging to decompose analytically into sky position and polar angle components, we suggest an alternative approach that entails the multiplication of the results derived from the pair of diagrams presented in Figure 3 to ascertain the response factor:

$$P_{res} = P(\lambda, \beta) \times P(\psi, \iota). \quad (13)$$

To verify the reliability of this calculation, we randomly sample 1,000 points to assess whether this approximation introduces any error. All sampled points fall within the detectable range of masses between $10^4 \sim 10^7 M_\odot$. As depicted in Figure 4, the 1σ relative error arising from this method remains well within an acceptable range of 2%.

IV. STELLAR-MASS BLACK HOLES

Besides MBHBs, we are further exploring the feasibility of deriving an analytical SNR formula for inspiral SBBHs. Due to the relatively high frequency at which SBBHs evolves within TianQin's sensitive band, the low-frequency approximation is no longer applicable. Conversely, the PSD formula of TianQin in ASA case can be

simplified as follows:

$$S_n = \frac{10}{3} L^2 S_p \times \left[1 + 0.6 \left(\frac{2\pi f L}{c} \right)^2 \right] \quad (14)$$

Using the same methodology of MBHB, we can obtain the SNR:

$$\begin{aligned} \rho(T_{\text{obs}}) &= \frac{1.15829}{c^{11/4} \sqrt{N_p}} (GM)^{5/4} \frac{L}{D_L} \times \left(\sqrt{t_c} - \sqrt{t_c - T_{\text{obs}}} \right)^{1/2} \\ &\approx 8.4 \left(\frac{\mathcal{M}}{100 M_\odot} \right)^{5/4} \frac{100 \text{ Mpc}}{D_L} \\ &\quad \times \left(\sqrt{\frac{t_c}{1 \text{ month}}} - \sqrt{\frac{t_c - T_{\text{obs}}}{1 \text{ month}}} \right)^{1/2}, \end{aligned} \quad (15)$$

and the lowest-order correction:

$$\begin{aligned} C &= -\frac{0.388101}{c^{13/3} N_p} (GM)^{5/3} \frac{L^{10/3}}{D_L^2} \times [\mathcal{F}(t_c) - \mathcal{F}(t_c - T_{\text{obs}})], \\ &\approx 162 \left(\frac{\mathcal{M}}{100 M_\odot} \right)^{5/3} \left(\frac{100 \text{ Mpc}}{D_L} \right)^2 \times [\mathcal{F}(t_c) - \mathcal{F}(t_c - T_{\text{obs}})], \end{aligned} \quad (16)$$

where,

$$\begin{aligned} \mathcal{F}(t) &= \arctan \left[0.57735 - \frac{0.577948 c^{7/12} L^{2/3}}{(GM)^{5/12} t^{1/4}} \right], \\ &\approx \arctan \left[0.57735 - \frac{0.23866}{\left(\frac{\mathcal{M}}{100 M_\odot} \right)^{5/12} \left(\frac{t}{1 \text{ month}} \right)^{1/4}} \right] \end{aligned} \quad (17)$$

In our test, as shown in Figure 5, we found that in the case of ASA, our formula provided good estimation accuracy for SBBHs. Without incorporating the lowest-order correction, we could make good estimates of the

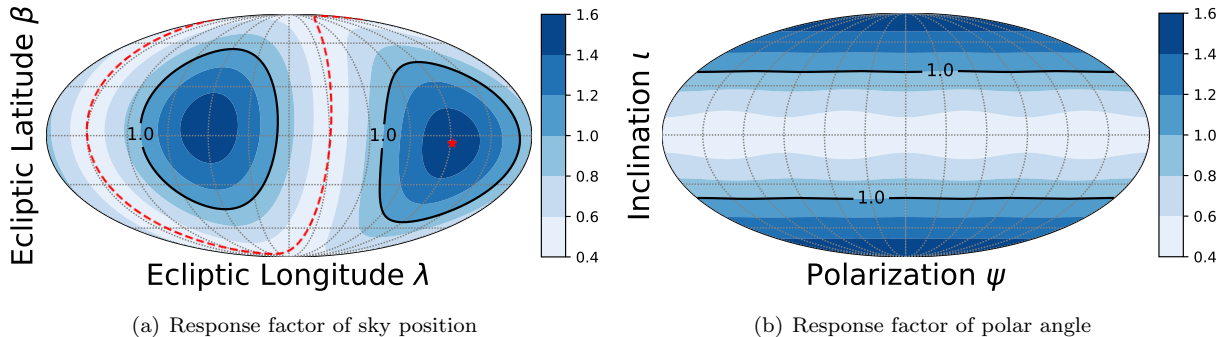


FIG. 3. The left panel illustrates the variation of the response factor with respect to sky position, with the TianQin orbit plane marked by a red dashed line and the position of the double white dwarf system RX J0806.3 + 1527 marked by a red asterisk, signifying the direction in which the TianQin constellation is pointed. The right panel depicts the variation of the response factor with respect to the polar angle. Both figures highlight where the response factor equals 1.0 with a black line.

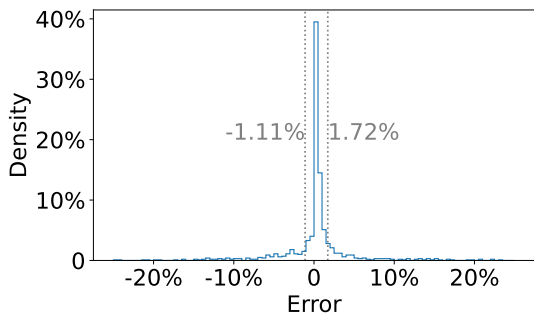


FIG. 4. The density plot of the relative error for Equation 13, calculated using 1,000 random scenarios. The 1σ error of the relative error is represented by a grey dotted line.

SNR for signals ranging from $5 \sim 500 M_{\odot}$. The SNR was overestimated for signals outside this range. When the lowest-order correction was applied, the SNR of most signals with masses below $500 M_{\odot}$ could be accurately calculated.

Despite our formula providing good estimations in the case of ASA, the SBBH signal with response is challenging to compute analytically. As illustrated in Figure 6, after considering the TDI response, the low-frequency component of the PSD remains smooth, allowing the SNR of the MBHB signal with response to be analytically approximated using low-frequency approximation. While in the high-frequency regime where SBBH resides, the PSD becomes highly complex and lacks a satisfactory formula for approximation. However, it is important to note that while we consider a three-month observation for all systems, SBBHs can keep inspiraling within the sensitive bands of space detectors for years. Therefore, our estimation of the ASA SNR will also be applicable for such long-duration inspiral-only observations.

V. CONCLUSION

In this work, we present a simplified analytic formula for the SNR of BBH systems in the context of TianQin. The analytical formula for low-frequency scenarios is applicable to signals from MBHBs with chirp masses above approximately $10^3 M_{\odot}$, while the analytical formula for high-frequency scenarios is suitable for signals from SBBHs with chirp masses below approximately $500 M_{\odot}$.

We evaluated the significance of errors resulting from using SNR analytical formulae. For TianQin, our formula of MBHB can accurately estimate the inspiral signals within the mass range of 10^3 to $10^4 M_{\odot}$. Incorporating a lowest-order correction can extend the range of accurate estimates between 10^3 and $10^5 M_{\odot}$. However, for LISA, achieving a good estimation accuracy is challenging, regardless of whether the lowest-order correction is considered.

Then, we derived an accurate analytical formula for the SNR of SBBHs in the ASA case. The formula can accurately estimate the inspiral signals within the mass range of 5 to $500 M_{\odot}$. Upon the application of the lowest-order correction, the SNR of the majority of signals with chirp mass below $500 M_{\odot}$ could be accurately calculated. Due to the complexity of the PSD at high frequencies, it remains challenging to provide a precise analytical formula for the SNR of SBBH signals with response. We will delve into this scenario in the future.

Specifically, we computed the SNR analytic formulae for both the ASA and non-average conditions. The sole discrepancy between these two scenarios is a coefficient, which we have termed the "response factor". This factor is exclusively affected by the sky position and the polar angle and does not vary over time. Despite the difficulty in performing an analytical calculation, we have developed a simple numerical approach to determine its value across different sky positions and polar angles. By sampling points over the parameter spaces including either the sky position or the polar angle and multiplying the

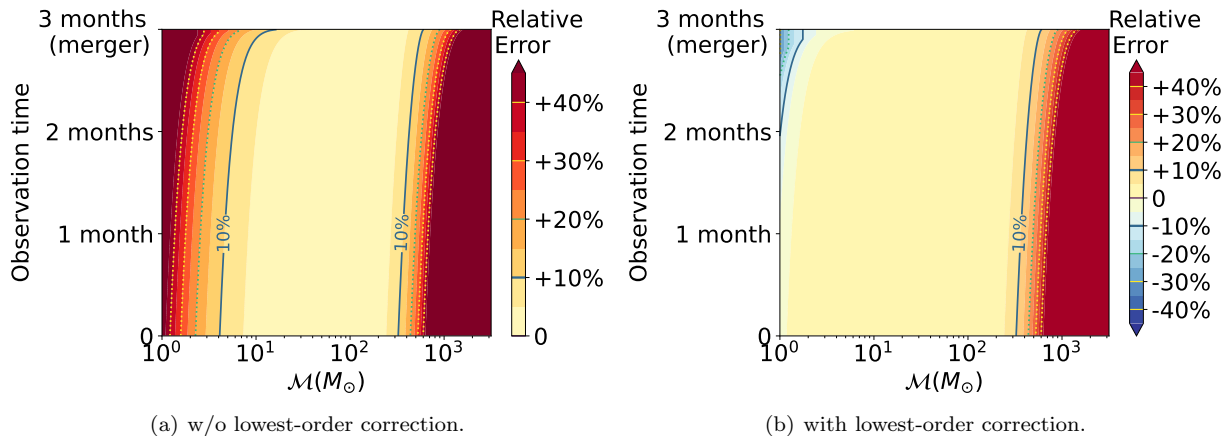


FIG. 5. The SNR estimation error of SBBHs for TianQin varies with the chirp mass and observation time. The left panel uses the simplest zeroth-order SNR formula for estimation, while the right panel considers the lowest-order correction.

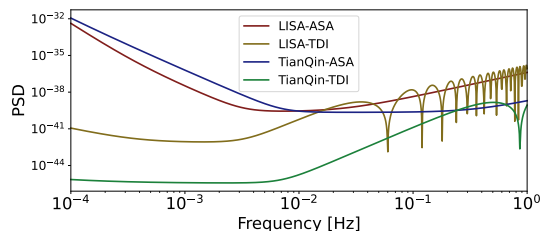


FIG. 6. The PSD curves of TianQin and LISA under ASA and TDI-A/E channel response conditions.

evaluated values, we obtain an approximate estimation result with an error margin of within 2%.

ACKNOWLEDGMENT

This work has been supported by the National Key Research and Development Program of China (No. 2023YFC2206700), and the Natural Science Foundation of China (Grants No. 12173104, No. 12261131504). We thank Jian-Wei Mei and Jian-Dong Zhang for their helpful comments.

-
- [1] LIGO Scientific Collaboration, J. Aasi, B. P. Abbott, R. Abbott, T. Abbott, M. R. Abernathy, et al., Advanced LIGO, *Class.Quant.Grav.* **32**, 074001 (2015), arXiv:1411.4547 [gr-qc].
 - [2] B. P. Abbott, R. Abbott, T. D. Abbott, M. R. Abernathy, F. Acernese, et al., GW150914: First results from the search for binary black hole coalescence with Advanced LIGO, *Phys.Rev.D* **93**, 122003 (2016), arXiv:1602.03839 [gr-qc].
 - [3] B. P. Abbott, R. Abbott, T. D. Abbott, M. R. Abernathy, F. Acernese, K. Ackley, et al., GW150914: The Advanced LIGO Detectors in the Era of First Discoveries, *Phys.Rev.Lett.* **116**, 131103 (2016), arXiv:1602.03838 [gr-qc].
 - [4] B. P. Abbott, R. Abbott, T. D. Abbott, S. Abraham, F. Acernese, et al., GWTC-1: A Gravitational-Wave Transient Catalog of Compact Binary Mergers Observed by LIGO and Virgo during the First and Second Observing Runs, *Physical Review X* **9**, 031040 (2019), arXiv:1811.12907 [astro-ph.HE].
 - [5] R. Abbott, T. D. Abbott, S. Abraham, F. Acernese, K. Ackley, et al., GWTC-2: Compact Binary Coalescences Observed by LIGO and Virgo during the First Half of the Third Observing Run, *Physical Review X* **11**, 021053 (2021), arXiv:2010.14527 [gr-qc].
 - [6] R. Abbott, T. D. Abbott, F. Acernese, K. Ackley, C. Adams, et al., GWTC-3: Compact Binary Coalescences Observed by LIGO and Virgo During the Second Part of the Third Observing Run, arXiv e-prints , arXiv:2111.03606 (2021), arXiv:2111.03606 [gr-qc].
 - [7] G. Agazie, A. Anumalapudi, A. M. Archibald, Z. Arzoumanian, P. T. Baker, et al., The NANOGrav 15 yr Data Set: Evidence for a Gravitational-wave Background, *The Astrophysical Journal Letters* **951**, L8 (2023), arXiv:2306.16213 [astro-ph.HE].
 - [8] J. Antoniadis, P. Arumugam, S. Arumugam, S. Babak, M. Bagchi, et al., The second data release from the European Pulsar Timing Array III. Search for gravitational wave signals, arXiv e-prints , arXiv:2306.16214 (2023), arXiv:2306.16214 [astro-ph.HE].
 - [9] D. J. Reardon, A. Zic, R. M. Shannon, G. B. Hobbs, M. Bailes, et al., Search for an Isotropic Gravitational-wave Background with the Parkes Pulsar Timing Array, *The Astrophysical Journal Letters* **951**, L6 (2023), arXiv:2306.16215 [astro-ph.HE].
 - [10] H. Xu, S. Chen, Y. Guo, J. Jiang, B. Wang, et al., Searching for the Nano-Hertz Stochastic Gravitational Wave Background with the Chinese Pulsar Timing Array Data Release I, *Research in Astronomy and Astrophysics* **23**, 075024 (2023), arXiv:2306.16216 [astro-ph.HE].

- [11] Y. Gong, J. Luo, and B. Wang, Concepts and status of Chinese space gravitational wave detection projects, *Nature Astron.* **5**, 881 (2021), arXiv:2109.07442 [astro-ph.IM].
- [12] J. Luo, L.-S. Chen, H.-Z. Duan, Y.-G. Gong, S. Hu, et al., TianQin: a space-borne gravitational wave detector, *Class.Quant.Grav.* **33**, 035010 (2016), arXiv:1512.02076 [astro-ph.IM].
- [13] E.-K. Li et al., Gravitational Wave Astronomy With TianQin, arXiv (2024), arXiv:2409.19665 [astro-ph.GA].
- [14] H.-T. Wang, Z. Jiang, A. Sesana, E. Barausse, S.-J. Huang, et al., Science with the TianQin observatory: Preliminary results on massive black hole binaries, *Phys.Rev.D* **100**, 043003 (2019), arXiv:1902.04423 [astro-ph.HE].
- [15] A. Sesana, J. Gair, E. Berti, and M. Volonteri, Reconstructing the massive black hole cosmic history through gravitational waves, *Phys.Rev.D* **83**, 044036 (2011), arXiv:1011.5893 [astro-ph.CO].
- [16] J. D. Schnittman, Astrophysics of super-massive black hole mergers, *Class.Quant.Grav.* **30**, 244007 (2013), arXiv:1307.3542 [gr-qc].
- [17] L.-G. Zhu, Y.-M. Hu, H.-T. Wang, J.-d. Zhang, X.-D. Li, et al., Constraining the cosmological parameters using gravitational wave observations of massive black hole binaries and statistical redshift information, *Phys.Rev.Res.* **4**, 013247 (2022), arXiv:2104.11956 [astro-ph.CO].
- [18] E. Berti, E. Barausse, V. Cardoso, L. Gualtieri, P. Pani, et al., Testing general relativity with present and future astrophysical observations, *Class.Quant.Grav.* **32**, 243001 (2015), arXiv:1501.07274 [gr-qc].
- [19] K. Yagi and L. C. Stein, Black hole based tests of general relativity, *Class.Quant.Grav.* **33**, 054001 (2016), arXiv:1602.02413 [gr-qc].
- [20] J. R. Gair, M. Vallisneri, S. L. Larson, and J. G. Baker, Testing General Relativity with Low-Frequency, Space-Based Gravitational-Wave Detectors, *Living Rev.Rel.* **16**, 7 (2013), arXiv:1212.5575 [gr-qc].
- [21] H.-Y. Chen, X.-Y. Lyu, E.-K. Li, and Y.-M. Hu, Near real-time gravitational wave data analysis of the massive black hole binary with TianQin, *Science China Physics, Mechanics, and Astronomy* **67**, 279512 (2024), arXiv:2309.06910 [gr-qc].
- [22] S. Liu, Y.-M. Hu, J.-d. Zhang, and J. Mei, Science with the TianQin observatory: Preliminary results on stellar-mass binary black holes, *Phys. Rev. D* **101**, 103027 (2020), arXiv:2004.14242 [astro-ph.HE].
- [23] R. Busicchio, A. Klein, E. Roebber, C. J. Moore, D. Gerosa, E. Finch, and A. Vecchio, Bayesian parameter estimation of stellar-mass black-hole binaries with LISA, *Phys. Rev. D* **104**, 044065 (2021), arXiv:2106.05259 [astro-ph.HE].
- [24] A. Nishizawa, E. Berti, A. Klein, and A. Sesana, eLISA eccentricity measurements as tracers of binary black hole formation, *Phys. Rev. D* **94**, 064020 (2016), arXiv:1605.01341 [gr-qc].
- [25] H. Wang, I. Harry, A. Nitz, and Y.-M. Hu, Space-based gravitational wave observatories will be able to use eccentricity to unveil stellar-mass binary black hole formation, *Phys. Rev. D* **109**, 063029 (2024), arXiv:2304.10340 [astro-ph.HE].
- [26] E. Barausse, N. Yunes, and K. Chamberlain, Theory-Agnostic Constraints on Black-Hole Dipole Radiation with Multiband Gravitational-Wave Astrophysics, *Phys. Rev. Lett.* **116**, 241104 (2016), arXiv:1603.04075 [gr-qc].
- [27] K. Kyutoku and N. Seto, Gravitational-wave cosmography with LISA and the Hubble tension, *Phys. Rev. D* **95**, 083525 (2017), arXiv:1609.07142 [astro-ph.CO].
- [28] K. Chamberlain and N. Yunes, Theoretical Physics Implications of Gravitational Wave Observation with Future Detectors, *Phys. Rev. D* **96**, 084039 (2017), arXiv:1704.08268 [gr-qc].
- [29] W. Del Pozzo, A. Sesana, and A. Klein, Stellar binary black holes in the LISA band: a new class of standard sirens, *Mon. Not. Roy. Astron. Soc.* **475**, 3485 (2018), arXiv:1703.01300 [astro-ph.CO].
- [30] C. Cutler and É. E. Flanagan, Gravitational waves from merging compact binaries: How accurately can one extract the binary's parameters from the inspiral waveform?, *Phys.Rev.D* **49**, 2658 (1994), arXiv:gr-qc/9402014 [gr-qc].
- [31] C. J. Moore, R. H. Cole, and C. P. L. Berry, Gravitational-wave sensitivity curves, *Class.Quant.Grav.* **32**, 015014 (2015), arXiv:1408.0740 [gr-qc].
- [32] L. Blanchet, Gravitational Radiation from Post-Newtonian Sources and Inspiralling Compact Binaries, *Living Rev.Rel.* **17**, 2 (2014), arXiv:1310.1528 [gr-qc].
- [33] S. Husa, S. Khan, M. Hannam, M. Pürrer, F. Ohme, et al., Frequency-domain gravitational waves from nonprecessing black-hole binaries. I. New numerical waveforms and anatomy of the signal, *Phys.Rev.D* **93**, 044006 (2016), arXiv:1508.07250 [gr-qc].
- [34] S. Husa, S. Khan, M. Hannam, M. Pürrer, F. Ohme, X. J. Forteza, and A. Bohé, Frequency-domain gravitational waves from nonprecessing black-hole binaries. I. New numerical waveforms and anatomy of the signal, *Physical Review D* **93**, 044006 (2016), arXiv:1508.07250 [gr-qc].
- [35] S. Khan, S. Husa, M. Hannam, F. Ohme, M. Pürrer, X. J. Forteza, and A. Bohé, Frequency-domain gravitational waves from nonprecessing black-hole binaries. II. A phenomenological model for the advanced detector era, *Physical Review D* **93**, 044007 (2016), arXiv:1508.07253 [gr-qc].
- [36] P. Amaro-Seoane, H. Audley, S. Babak, J. Baker, E. Barausse, et al., Laser Interferometer Space Antenna, arXiv e-prints, arXiv:1702.00786 (2017), arXiv:1702.00786 [astro-ph.IM].
- [37] E.-K. Li, H. Wang, H.-Y. Chen, H. Fan, Y.-N. Li, Z.-Y. Li, et al., GWSpace: a multi-mission science data simulator for space-based gravitational wave detection, arXiv e-prints, arXiv:2309.15020 (2023), arXiv:2309.15020 [gr-qc].
- [38] E. Poisson, Gravitational radiation from a particle in circular orbit around a black hole. 1: Analytical results for the nonrotating case, *Phys. Rev. D* **47**, 1497 (1993).
- [39] M. Vallisneri, Synthetic LISA: Simulating time delay interferometry in a model LISA, *Phys.Rev.D* **71**, 022001 (2005), arXiv:gr-qc/0407102 [gr-qc].
- [40] S. Marsat, J. G. Baker, and T. D. Canton, Exploring the Bayesian parameter estimation of binary black holes with LISA, *Phys.Rev.D* **103**, 083011 (2021), arXiv:2003.00357 [gr-qc].

Appendix A: Detectors Setting

For TianQin[12, 37], the arm length $L = \sqrt{3} \times 10^8$ m. The residual acceleration noise S_a of the test masses in the satellites, and the position measurement noise S_p can be represented as:

$$S_a = N_a \times \left(1 + \frac{10^{-4} \text{ Hz}}{f}\right), \quad (\text{A1})$$

$$S_p = N_p, \quad (\text{A2})$$

where, $N_a = 10^{-30} \text{ m}^2/\text{s}^4/\text{Hz}$, $N_p = 10^{-24} \text{ m}^2/\text{Hz}$.

For LISA[36, 37], the arm length $L = 2.5 \times 10^9$ m. S_a and S_p can be represented as:

$$S_a = N_a \times \left[1 + \left(\frac{0.4 \times 10^{-3} \text{ Hz}}{f}\right)^2\right] \times \left[1 + \left(\frac{f}{8 \times 10^{-3} \text{ Hz}}\right)^4\right], \quad (\text{A3})$$

$$S_p = N_p \times \left[1 + \left(\frac{2 \times 10^{-3} \text{ Hz}}{f}\right)^4\right]. \quad (\text{A4})$$

where, $N_a = 9 \times 10^{-30} \text{ m}^2/\text{s}^4/\text{Hz}$, $N_p = 2.25 \times 10^{-22} \text{ m}^2/\text{Hz}$.

Moreover, TianQin is only sensitive to signals at the frequency range of $f_{\text{low}} = 10^{-4}$ Hz to $f_{\text{high}} = 1$ Hz. Consequently, any signal outside this range should be truncated. For low-frequency cutoff, we discard data before t_l :

$$t'_c = t_c - t_l, \quad T'_{\text{obs}} = T_{\text{obs}} - t_l, \quad \text{if } t_l > 0, \quad (\text{A5})$$

$$t'_c = t_c, \quad T'_{\text{obs}} = T_{\text{obs}}, \quad \text{if } t_l \leq 0. \quad (\text{A6})$$

For high-frequency cutoff, we discard data after t_h :

$$T'_{\text{obs}} = \min\{T_{\text{obs}}, t_h\}, \quad (\text{A7})$$

where, the t_l and t_h can be calculated from Equation 5:

$$t_l = t_c - \frac{5}{(8\pi f_{\text{low}})^{8/3}} \left(\frac{GM}{c^3}\right)^{-5/3},$$

$$\approx t_c - 18 \text{ h} \times \left(\frac{10^7 M_{\odot}}{\mathcal{M}}\right)^{5/3}. \quad (\text{A8})$$

$$t_h = t_c - \frac{5}{(8\pi f_{\text{high}})^{8/3}} \left(\frac{GM}{c^3}\right)^{-5/3},$$

$$\approx t_c - 180 \text{ h} \times \left(\frac{1 M_{\odot}}{\mathcal{M}}\right)^{5/3}. \quad (\text{A9})$$

Appendix B: ASA SNR with low-frequency approximation

The GWs emitted by BBH systems can be described by multiple modes, each corresponding to different oscillation patterns as the waves propagate through space-time. These modes are often classified by their angular

harmonics, denoted by the symbol (l, m) representing the multipole moment of the wave. The quadrupole 22 mode, with $l = m = 2$, is the most significant and typically the only feature in the GW signal observed at large distances from the source. Therefore, in this work, we only consider GWs produced by the 22 mode. Consequently, in ASA condition, the coefficients of the 22 mode [38] will be retained:

$$\mathcal{A}_{ASA}(f) = \sqrt{\frac{5}{16\pi}} \times \mathcal{A}(f). \quad (\text{B1})$$

Additionally, the ASA sensitivity curve of TianQin can be represented as [37]:

$$S_n = \frac{10}{3} \frac{1}{L^2} \left[\frac{4S_a}{(2\pi f)^4} + S_p \right] \times \left[1 + 0.6 \left(\frac{f}{f_*}\right)^2 \right], \quad (\text{B2})$$

where $f_* \equiv c/(2\pi L) \approx 0.28$ Hz.

Given that the inspiral signals from MBHBs are generally found in the low-frequency spectrum with $f \ll f_*$, the S_p and $[1 + 0.6(f/f_*)^2]$ terms of the Equation B2, which primarily influence high frequencies, can be omitted. Besides, we can firstly assume that the residual acceleration noise $S_a = N_a$ is frequency-independent, and then the sensitivity curve of TianQin can be approximated as:

$$S_n \simeq \frac{5}{6\pi^4} \frac{1}{L^2} N_a f^{-4} \quad (\text{B3})$$

By combining the amplitude (Equation B1) and sensitivity curve (Equation B3) under the ASA condition, we can calculate the square of the SNR:

$$\rho^2 = 4 \int_{f_{\text{min}}}^{f_{\text{max}}} \frac{\mathcal{A}_{ASA}^2(f)}{S_n(f)} df,$$

$$= \frac{\pi^{8/3}}{c^3} \left(\frac{L}{D_L}\right)^2 \frac{1}{N_a} (GM)^{5/3} \int_{f_{\text{min}}}^{f_{\text{max}}} f^{5/3} df,$$

$$= \frac{15c^2}{2048 N_a t_c} \left(\frac{L}{D_L}\right)^2 \frac{T_{\text{obs}}}{t_c - T_{\text{obs}}}, \quad (\text{B4})$$

It is of particular interest to observe that within this SNR formula, all elements associated with mass, originating from both the time-frequency relation and the amplitude, have been effectively eliminated.

By extracting the square root of the aforementioned equation, we derive the relationship that governs the accumulation of SNR over time:

$$\rho(T_{\text{obs}}) = \sqrt{\frac{15}{2048}} \frac{L}{D_L} \frac{c}{\sqrt{N_a t_c}} \times \sqrt{\frac{t_{\text{obs}}}{t_c - t_{\text{obs}}}},$$

$$\approx 185.2 \times \frac{1 \text{ Gpc}}{D_L} \sqrt{\frac{1 \text{ week}}{t_c}} \times \sqrt{\frac{T_{\text{obs}}}{t_c - T_{\text{obs}}}}. \quad (\text{B5})$$

Appendix C: Calculation of the response factor

The response of a space-based GW detector can be characterized by the single-link observables, represented

as $y_{slr} = (\nu_r - \nu_s)/\nu$, which quantifies the relative laser frequency shift between the transmitting spacecraft (s) and the receiving spacecraft (r) along the link (l) [37, 39, 40]. The relationship between the observable and the source waveform is described by:

$$\tilde{y}_{slr} = G_{slr}^{22}(f, t) \times \mathcal{A}e^{i\Phi}, \quad (\text{C1})$$

where, Φ is the waveform phase, and $G_{slr}^{22}(f, t)$ denotes the transfer function [37, 40]:

$$G_{slr}^{22}(f, t) = -\frac{i\pi fL}{2c} \times \text{sinc}\left[\frac{\pi fL}{c}(1 - k \cdot n_l)\right] \times \exp\left[i\pi f\left(\frac{L + k \cdot (p_r + p_s)}{c}\right)\right] \times P_{slr}(t), \quad (\text{C2})$$

with k representing the wave propagation vector, and s, r denoting the transmitting and receiving spacecraft, respectively. The expression $P_{slr}(t) = n_l(t) \cdot P^{22} \cdot n_l(t)$ defines the inner product of the 2-2 mode polarization tensor P^{22} and the link unit vectors n_l .

By eliminating the phase terms that do not affect the SNR and employing a low-frequency approximation, the amplitude of the observable can be simplified as:

$$\tilde{y}_{slr} \simeq -\frac{i\pi fL}{2c} \times P_{slr}(t) \times \mathcal{A}, \quad (\text{C3})$$

Here we employ the standard set of orthogonal TDI observables, namely A, E, and T. The waveforms in these channels can be expressed as [37, 40]:

$$\tilde{A}, \tilde{E} = i\sqrt{2} \sin\left(\frac{f}{f_*}\right) \exp\left(i\frac{f}{f_*}\right) \times \tilde{a}, \tilde{e}, \quad (\text{C4})$$

$$\tilde{T} = 2\sqrt{2} \sin\left(\frac{f}{f_*}\right) \sin\left(\frac{f}{2f_*}\right) \exp\left(i\frac{3f}{2f_*}\right) \times \tilde{t}, \quad (\text{C5})$$

where the \tilde{a} , \tilde{e} and \tilde{t} terms can be simplified, under the low-frequency approximation, to [40]:

$$\tilde{a} \simeq 4\tilde{y}_{31} - 2\tilde{y}_{23} - 2\tilde{y}_{12}, \quad (\text{C6})$$

$$\tilde{e} \simeq 2\sqrt{3}[\tilde{y}_{12} - \tilde{y}_{23}], \quad (\text{C7})$$

$$\tilde{t} \simeq 0. \quad (\text{C8})$$

Therefore, the absence of signals in the T-channel data does not contribute to the SNR. Meanwhile, the signal in the A and E channels can be further simplified as:

$$\tilde{A} \simeq 2\sqrt{2}\mathcal{A}\left(\frac{\pi fL}{c}\right)^2 (2P_{31} - P_{23} - P_{12}), \quad (\text{C9})$$

$$\tilde{E} \simeq 2\sqrt{6}\mathcal{A}\left(\frac{\pi fL}{c}\right)^2 (P_{12} - P_{23}). \quad (\text{C10})$$

Additionally, the noise PSD in the A, E channels can be represented as [37]:

$$S_A = S_E = 8 \sin^2\left(\frac{f}{f_*}\right) \left[4 \left(1 + \cos\left(\frac{f}{f_*}\right) + \cos\left(2\frac{f}{f_*}\right) \right) S_{\text{acc}} + \left(2 + \cos\left(\frac{f}{f_*}\right) \right) S_{\text{oms}} \right], \quad (\text{C11})$$

where $S_{\text{acc}} = S_a (1/(2\pi fc))^2$ is the acceleration noise, primarily dominant at low frequencies. And $S_{\text{oms}} = S_p ((2\pi f)/c)^2$ is the displacement or position noise, primarily dominant at high frequencies. Therefore, after also applying the low-frequency approximation and the frequency-independent S_a approximation, the low-frequency TDI noise PSD of TianQin can be simplified to:

$$S_A = S_E \simeq \frac{96 S_a L^2}{c^4} \simeq \frac{96 N_a L^2}{c^4}. \quad (\text{C12})$$

Ultimately, using the signals (Equation C9, C10) and noise PSD (Equation C12) in the A and E channels, we can calculate the SNR for MBHBs in non-average scenarios:

$$\rho^2 = 4 \int_{f_{\min}}^{f_{\max}} \frac{\tilde{A}^2(f) + \tilde{E}^2(f)}{S_A} df, \simeq \frac{\pi^{8/3}}{2c^3} \left(\frac{L}{D_L}\right)^2 \frac{1}{N_a} (GM)^{5/3} \int_{f_{\min}}^{f_{\max}} P_{\text{res}}^2 f^{5/3} df, \quad (\text{C13})$$

where, the response factor P_{res} is defined as:

$$P_{\text{res}}^2 = \frac{8\pi}{9} \times (P_{12}^2 + P_{23}^2 + P_{31}^2 - P_{12}P_{31} - P_{23}P_{31} - P_{12}P_{23}). \quad (\text{C14})$$

It is noteworthy that, although each P_{slr} fluctuates with time and frequency, the aggregation into P_{res} form renders it temporally invariant, with variation contingent only upon the sources' sky positions and polar angles. This enables the extrication of this term from the integral, thereby maintaining the simplicity of the SNR formulation. Consequently, the SNR formula in the non-average form simply incorporates an extra P_{res} term compared to the ASA form (Equation 7):

$$\rho(T_{\text{obs}}) \simeq \sqrt{\frac{15}{2048}} \frac{L}{D_L} \frac{c}{\sqrt{N_a t_c}} P_{\text{res}} \times \sqrt{\frac{T_{\text{obs}}}{t_c - T_{\text{obs}}}}, \quad (\text{C15})$$